Response of tropical cyclone potential intensity over the north Indian Ocean to global warming

Jinhua Yu[1,2] and Yuqing Wang[2]

Received 20 November 2008; revised 2 January 2009; accepted 22 January 2009; published 14 February 2009.

[1] The responses of tropical cyclone (TC) potential intensity (PI) and the associated environmental control parameters over the North Indian Ocean (NIO) to the doubled CO_2 concentration are assessed based on the ensemble simulation from 15 coupled general circulation models (CGCMs) participated in the Intergovernmental Panel for Climate Change (IPCC) Forth Assessment Report (AR4). The results show that the annual mean sea surface temperature (SST) averaged over the NIO increases 1.71°C. The thermodynamic efficiency changes little because the outflow layer temperature increases accordingly. The monthly mean vertical shear decreases across the NIO with a maximum decrease of 8% in May–June except for a small increase in April. The dynamic efficiency decreases to the north of 10°N over Bay of Bengal while increases significantly in the southern NIO in response to the doubled CO_2 concentration. The PI increases by 4.6% and 5.9% averaged over Arabian Sea and 2.0% and 4.86% averaged over Bay of Bengal during TC and summer monsoon seasons, respectively. An important finding is the significant increase in PI in May when the background PI is already high and the potentially longer TC season in response to global warming due to the decrease in vertical shear in June and September. **Citation:** Yu, J., and Y. Wang (2009), Response of tropical cyclone potential intensity over the north Indian Ocean to global warming, *Geophys. Res. Lett.*, *36*, L03709, doi:10.1029/2008GL036742.

1. Introduction

[2] Tropical Storm Nargis (2008) formed in the North Indian Ocean (NIO) and landed in Burma in early May 2008. With its maximum low-level wind speed over 60 m s^{-1}, Nargis caused at least 146,000 fatalities and over $10 billion economic loss, the worst record in Burma. The sea surface temperature (SST) over the NIO has increased 0.6°C since 1960, the largest warming among the tropical oceans. A natural question arises as to whether the recent increase in frequency of severe tropical cyclones (TCs), such as Nargis, is related to the increase in SST in response to the increase in greenhouse gases. In addition to the increase in SST, the large-scale circulation over the NIO is also changing, leading to longer season in TC activity in the basin [*Rao et al.*, 2008]. *Rao et al.* [2008] indicate that tropical easterly jet (TEJ) associated with Asian summer monsoon over the NIO is weakening in recent years, which reduces the easterly vertical shear and thus is favorable for the formation of more severe tropical storms. If the present decreasing trend of TEJ intensity continues, there could be a strong likelihood of the formation of intense TCs even in the summer monsoon season.

[3] The potential intensity (PI) of TCs is an upper bound of the intensity that a TC may reach under a given environmental thermodynamic and dynamical conditions. Previous studies have indicated that the PI agrees well with the observed maximum intensities of most severe tropical storms and that the spatial and seasonal variability of real TC intensity is highly correlated to the variability of the PI determined by the environment [*Tonkin et al.*, 2000; *Bister and Emanuel*, 2002; *Free et al.*, 2004]. Assuming that these observed connections between the realized TC intensity and the PI hold in a changing climate, the predicted/projected PI should be a useful indication of how TC intensities would change with global warming [*Emanuel*, 2007]. Previous studies have shown how PI may change in future climate over the North Atlantic and Pacific based on thermodynamic control of PI [*Vecchi and Soden*, 2007].

[4] This study explores the model-projected increase in TC PI and the corresponding changes in the environmental thermodynamic and dynamical control parameters over the NIO. The monthly mean data based on the simulations from the most commonly used 15 coupled general circulation models (CGCMs) are used as the input parameters for the PI calculations. They are CCMA CGCM3, CNRM CM3, CSIRO MK3_5, GFDL CM2_0, GFDL CM2_1, GISS EH, GISS ER, IAP FGOALS1, INGV_ECHAM4, IPSL CM4, MIROC_HIRES, MIROC_MEDRES, MPIECHAM5, MRICGCM2, UKMOHADCM3, and UKMOHADGEM1. These models are forced by emission scenario 1pctto2x with CO_2 concentration increases at 1% per year to doubling in the 70th year and then fixed for the remainder of the run in the Intergovernmental Panel of Climate Change (IPCC) Fourth Assessment Report (AR4) experiments. We expect to gain insight into the possible changes in the activity of TCs in the NIO under a warmed climate.

2. Calculation of Potential Intensity

[5] The monthly mean SST, wind, temperature and specific humidity from 15 CGCMs selected in this study were downloaded from the website of the Program of Climate Model Diagnosis and Intercomparison (PCMDI) for IPCC-

[1]Pacific Typhoon Research Center, KLME, Nanjing University of Information Science and Technology, Nanjing, China.
[2]International Pacific Research Center and Department of Meteorology, School of Ocean and Earth Science and Technology, University of Hawaii at Manoa, Honolulu, Hawaii, USA.

0094-8276/09/2008GL036742$05.00

AR4/CMIP3 archive. The PI defined as low-level maximum wind speed of a TC in each month at each grid point for each model was calculated by

$$\mathrm{PI} = \eta \bullet \sqrt{\frac{T_S}{T_0}\frac{C_k}{C_D}\left[CAPE^* - CAPE\right]_m} \quad (1)$$

where T_s is the SST; T_0 is the outflow layer temperature; C_k is the exchange coefficient for enthalpy and C_D is the drag coefficient; *CAPE** is the convective available potential energy of air saturated at SST and lifted from sea level in reference to the environmental sounding; and *CAPE* is the convective available potential energy of boundary layer air. The subscript "m" indicates the values evaluated near the radius of maximum wind. In our calculation, we take $\frac{C_k}{C_D} = 0.8$. In equation (1), η is the dynamical efficiency, which takes into account the combined effect of vertical shear and translational speed and is empirically determined following *Zeng et al.* [2007]

$$\eta = \frac{1}{1 + U_{ST}/U_0} \quad (2)$$

where

$$U_{ST} = \sqrt{0.6V_{shear}^2 + (V_{trans} - 5)^2} \quad (3)$$

where V_{shear} is the vertical wind shear defined as the difference of wind speeds between 200 hPa and 850 hPa, and V_{trans} is the translational speed of the targeted TC, which is estimated in this study by the mass weighted wind speed between 850 hPa and 300 hPa. The dynamical efficiency indicates the negative effects of both vertical shear and translational speed [*Zeng et al.*, 2007]. $U_0 = 60$ m s^{-1}. The thermodynamic efficiency is defined as [*Emanuel*, 1999; *Bister and Emanuel*, 1998, 2002; *Zeng et al.*, 2007]

$$\varepsilon = \sqrt{\frac{SST - T_0}{T_0}} \quad (4)$$

which is a function of SST and the outflow layer temperature T_0. Note that if the dynamical efficiency is set to unit, equation (1) will become the thermodynamic PI developed by *Emanuel* [1999] and *Bister and Emanuel* [1998, 2002], which is determined by thermodynamic factors only. Therefore, the PI discussed in this study includes both thermodynamic and dynamical controls. In our analysis below, we will focus on the changes contributed by the linear trend in response to the doubled CO_2 concentration, which explains over 70% of the variance in the total PI changes.

3. Projected Change in Seasonal Variation of PI

[6] The ensemble-mean PI is the simple mean of PIs calculated using equation (1) for each grid point in each month from individual CGCMs over the NIO. Figure 1 shows the seasonal variation of the monthly mean background PI (which is defined as the first year value in the linear fitting for the transient response) and its relative change (in percentage) in the linear trend in response to the doubled CO_2 concentration and those of the associated control parameters averaged over the NIO (50°∼100°E, 5∼20°N). Large monthly mean background PI occurs in April–May and October–November with the highest PI of 62 m s^{-1} in April and November (Figure 1a). June–September shows the lowest PI, with 41 m s^{-1} in August, which corresponds to the summer monsoon season. The seasonal variation of PI is consistent with the seasonal variation of actual TC intensity in the basin [*Rao et al.*, 2008]. The PI averaged in the NIO increases by 2.9 to 6.3% in response to the doubled CO_2 concentration, depending strongly on season (Figure 1a). The increase in PI has an opposite tendency to the background PI in seasonal time scale. Large increases in PI (4.4%–6.3%) occur in JJA, namely, in the summer monsoon season with relatively low background PI. Small PI increases (2.9% and 3.1%) occur in the active TC seasons of April and November when the background PI is the largest. The PI change due to the linear trend explains over 70% variance of the total PI change in all months in response to the doubled CO_2 concentration and is statistically significant over 95% confidence levels. Therefore, the linear trend in PI change is the most important component in response to the global warming due to the increasing CO_2. From Figure 1b, one can see that the PI increases in all months as the CO_2 increases. This suggests not only a possible increase of severe tropical storms but also a potential longer duration of the active TC seasons in the NIO. This seems to be consistent with recent observational studies [*Webster et al.*, 2005; *Elsner et al.*, 2008; *Rao et al.*, 2008].

[7] The monthly mean background SST averaged over the NIO is warmer than 27°C from March to December (Figure 2a). It shows two peaks in the pre- and post-summer monsoon seasons, namely, around May and October, respectively, which correspond to the two valleys in outflow layer temperature (Figure 2b). The high SST together with the low outflow layer temperature leads to the relatively high background thermodynamic efficiency (Figure 2c) and CAPE (Figure 2d) in the two TC seasons. The monthly mean background vertical shear is quite strong (over 20 m s^{-1}) in the summer monsoon season during June–September and is generally around 10 m s^{-1} in April–May and October–November (Figure 2e). Large background vertical shear in the summer monsoon season leads to the smallest dynamical efficiency (0.73, Figure 2f), which partially contributes to the low PI and prohibits the formation of strong TCs in the summer monsoon season.

[8] To identify the dominant controls of the PI over the NIO, the correlation coefficients between various background control parameters and the background PI are calculated. The correlation coefficients between the monthly mean background PI and SST, outflow layer temperature, thermodynamic efficiency, CAPE, vertical shear, and dynamic efficiency are, respectively, 0.40, −0.77, 0.62, 0.96, −0.93 and 0.94 on seasonal time scale. This indicates that the seasonal variation of the background CAPE, dynamical efficiency contribute positively to the background PI, while the outflow layer temperature and vertical shear contribute negatively to the development and intensification of severe tropical storms. Note that SST is not highly correlated with

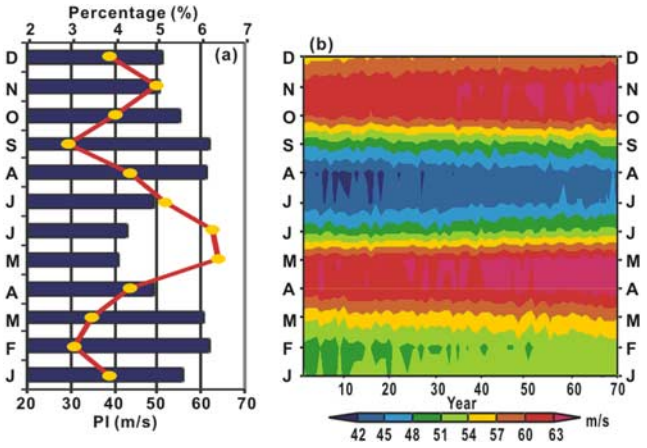

Figure 1. (a) Seasonal variation of ensemble monthly mean background PI (bars, first year in the linear fitting) and its change in percentage in response to doubled CO_2 concentration (curve, the relative changes between the 70th year and the first year) averaged over the NIO basin (50–100°E, 5–20°N); (b) the transient response of the basin-averaged PI to increasing CO_2 concentration.

the PI compared with CAPE and dynamical efficiency, indicating that SST is not the only control parameter to the PI since it is generally over 27°C from March to December in the basin (Figure 2a).

[9] Figure 2 also shows the basin-averaged changes of the corresponding thermodynamic and dynamical control parameters in the linear trends in response to the doubled CO_2 concentration. The SST increases year-round with the largest increase of 1.78°C in June and the lowest increase of 1.68°C in January and March (Figure 2a). The outflow layer temperature averaged over the NIO also increases year-round with the largest increase of 1.44°C in May and lowest increase of 0.21°C in February (Figure 2b). The thermodynamic efficiency (Figure 2c) thus shows a slight increase except for a small decrease in May–June and October, which has an opposite tendency to the outflow layer temperature (Figure 2c versus Figure 2b). The CAPE increases by 6%–9% with the maximum increase in the monsoon season (Figure 2d). Note that CAPE in this study is defined as the difference between the saturation CAPE* and the environmental CAPE at the radius of maximum wind. Therefore the CAPE is controlled by both SST and the vertical structure of temperature and humidity in the environment. Except for April and December, the vertical shear shows the largest decrease (8%) in May and June (Figure 2e), which is responsible for the increase of 1.6% in the dynamical efficiency in June (Figure 2f). The increase in vertical shear in April contributes to a decrease in dynamical efficient in the month, indicating the negative effect of vertical shear on the dynamical efficiency. The correlation coefficients between the changes in SST, outflow layer temperature, thermodynamic efficiency, CAPE, vertical

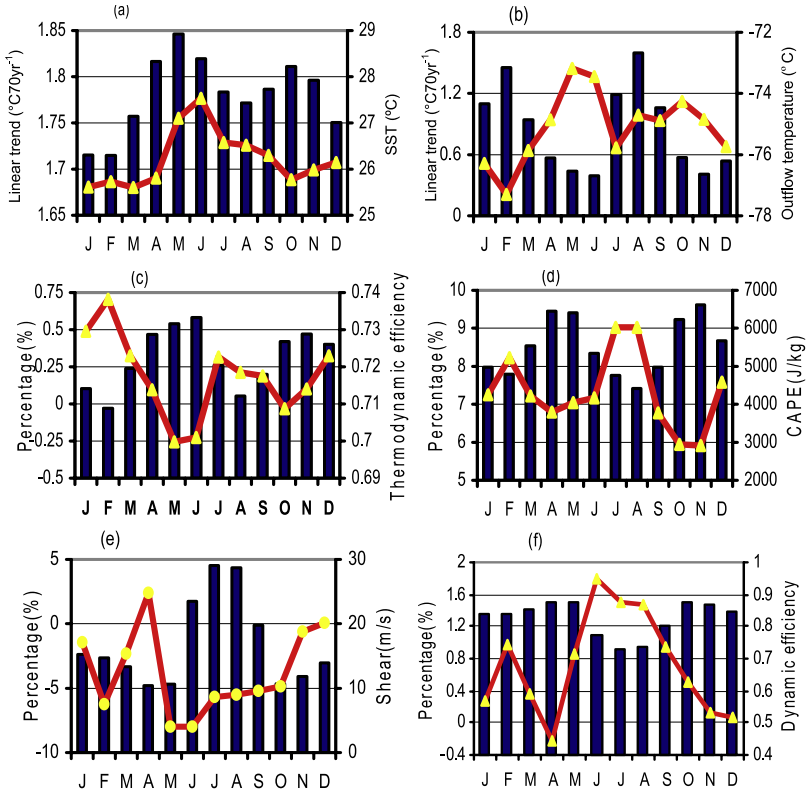

Figure 2. Seasonal variation of monthly ensemble-mean background thermodynamic and dynamical control parameters (bars, the first year background) and their relative changes in percentage (change between the 70th year and the first year relative to the first year background) in the linear trends in response to the doubled CO_2 concentration (curves): (a) SST (°C), (b) outflow layer temperature (°C), (c) thermodynamic efficiency, (d) CAPE (J/kg), (e) vertical shear between 200 hPa and 850 hPa (m s^{-1}), and (f) dynamical efficiency, all averaged over the North Indian Ocean (50–100°E, 5–20°N).

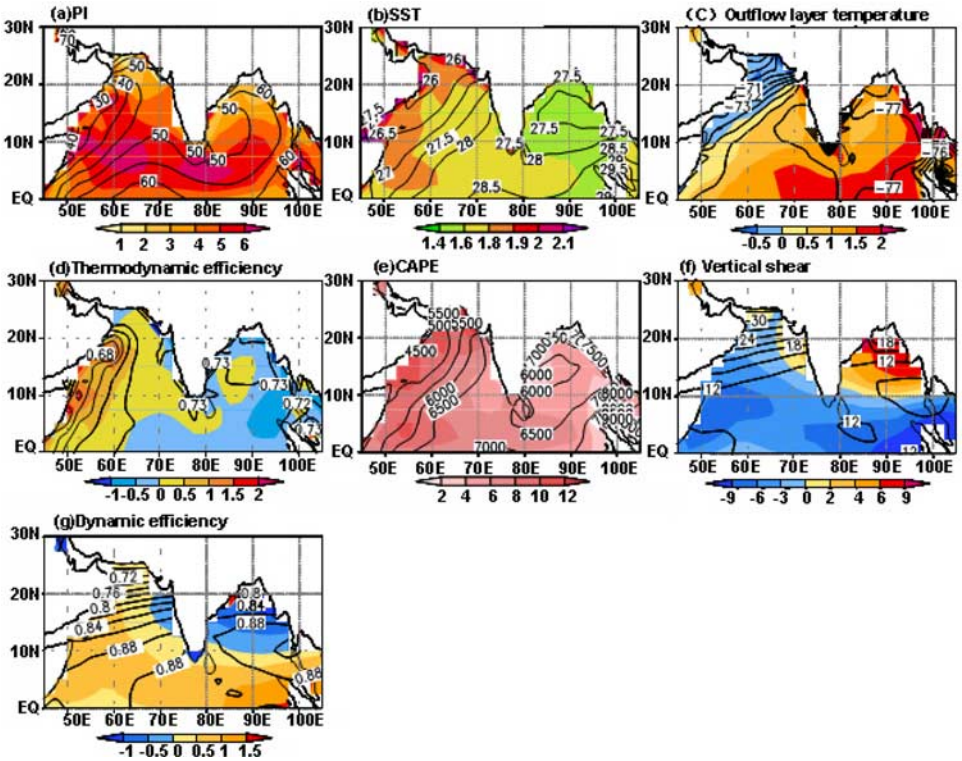

Figure 3. Spatial distribution of changes in PI of TCs and the associated large-scale environmental thermodynamic and dynamical parameters during TC season in response to the doubled CO_2 concentration based on 15 CGCM ensemble mean: (a) PI, (b) SST (°C), (c) outflow layer temperature (°C), (d) thermodynamic efficiency, (e) CAPE (J kg^{-1}), (f) vertical shear (m s^{-1}), (g) dynamical efficiency. Figures 3b and 3c show the change in linear trend, Figures 3a, 3d, 3e, 3f, and 3g show the relative changes (%) related to the background field. Contours show the corresponding background fields based on the same 15 CGCM model ensemble mean.

shear, and dynamical efficiency and that of the PI are, respectively, 0.51, −0.053, 0.13, 0.87, −0.67, and 0.89, indicating again that the seasonal variation in CAPE and dynamical efficiency control largely the change in PI in the NIO in response to the doubled CO_2 concentration.

4. Spatial Distribution of PI in TC Season

[10] There are two main basins in the NIO, namely, Arabian Sea to the west of the Indian subcontinent and Bay of Bengal (BoB) to the east. Severe TCs occur only in pre- (April–May) and post-monsoon (October–November) seasons (known as TC season in the NIO) when the vertical shear is weak. Figure 3 shows the spatial distribution of the background PI and the change of PI in the linear trend and its control parameters in response to the doubled CO_2 concentration during the TC season (April–May and October–November). Clearly, the background PI (Figure 3a) shows the spatial pattern very similar to that of the background SST, thermodynamic efficiency, and CAPE (Figure 3a versus Figures 3b, 3d, and 3e). The background PI in BoB (78°–100°E, 5°–20°N) is higher than in Arabian sea (50°–78°E, 5°–20°N) (Figure 3a). The PI shows a consistent increase across the NIO in response to the doubled CO_2 concentration. However, the increase in PI has an opposite east-west gradient to the background PI, with less increase in BoB (1.32 m s^{-1} or by 2% on average) than in Arabian Sea (2.63 m s^{-1} or 4.6% on average) during the TC season (Figure 3a). This spatial distribution in PI change is consistent with the local trends in SST, CAPE and dynamical efficiency (Figure 3a versus Figures 3b, 3e, and 3g), indicating the dominant control of the PI response to the doubled CO_2 concentration by the local SST, CAPE, and dynamical efficiency. As we can see from Figure 3b, SST increases in the whole basin (1.34–2.34°C) in response to the doubled CO_2, with larger increase in Arabian Sea (averaged 1.79°C), especially near its northwest coast, than in BoB (averaged 1.57°C) during TC season (Figure 3b). The largest increase in outflow layer temperature occurs in the southeast BoB, which is larger than the increase in SST (Figure 3c versus Figure 3b), resulting in a decrease in thermodynamic efficiency across most region of BoB while an increase in Arabian sea (Figure 3d, over 90% significance level in most areas) during TC season.

[11] The background vertical shear averaged in the NIO is about 12.06 m s^{-1} and with smaller shear in BoB (11.33 m s^{-1}) and larger shear in Arabian Sea (12.9 m s^{-1}) during TC season (Figure 3). In the monsoon season (July–September), the background vertical shear is 25 m s^{-1} on average with the largest shear over 30 m s^{-1} around 10°N. Strong vertical shear is responsible for few severe tropical storms in the monsoon season in the basin. The projected change in vertical shear in response to the doubled CO_2 concentration varies across the NIO and among different seasons. The vertical shear decreases by 6% averaged over the NIO basin with the largest decrease of 10.3% around

5°N over Arabian Sea during June–September (figure not shown) while it increases north of 10°N over the BoB and the northeast coast of Arabian Sea with the largest increase of 10%. More than 10% decrease in vertical shear occurs south of 10°N over BoB and most of the regions in Arabian Sea during the TC season (Figure 3f). The background dynamical efficiency averaged in the NIO is 0.86 and 0.74 in the TC season and monsoon season, respectively. Change in the dynamical efficiency shows opposite sign to the change in vertical shear (Figure 3g versus Figure 3f), indicating the negative effect of large-scale vertical shear on the dynamical efficiency. This negative effect can also be seen from Figure 3a where the smaller increase in PI coincides with larger increase in vertical shear or vice versa.

5. Conclusion

[12] This study analyzes the transient response of TC PI and its associated thermodynamic and dynamical control parameters to the global warming scenario due to the increase in CO_2 concentration using the ensemble mean of the projected simulations from the 15 CGCMs participated in IPCC-AR4. The results show that the annual mean SST averaged over the North Indian Ocean in response to the doubled CO_2 concentration increases 1.71°C with the maximum increase of 1.78°C in June and the minimum of 1.68°C in January. The SST increase in Bay of Bengal is smaller than that in Arabian Sea, especially in the TC season. The outflow temperature increases in response to the doubled CO_2 with a maximum increase of 1.44°C in May and a minimum of 0.21°C in February. The different spatial distribution in the changes in SST and outflow layer temperature results in a small decrease in thermodynamic efficiency across a large portion of Bay of Bengal while an increase over most of the Arabian Sea. The monthly mean vertical shear decreases by 5–8% averaged over NIO during May–September while increases north of 10°N over the Bay of Bengal in the TC season. The dynamical efficiency has an opposite trend to that of vertical shear. The seasonal variation of the background PI is correlated closely to that of CAPE and dynamical efficiency while weakly to that of SST, indicating that the background SST has a weak control on the development of severe tropical storms over the NIO. This may be partly due to the relatively high SST year round in the basin. The spatial pattern of the linear trend in PI during the TC season bears similarities to that of the linear trends in SST, CAPE, and dynamical efficiency, indicating that both dynamical and thermodynamic controls are important to the PI response to the doubled CO_2 concentration in the basin. The PI increases 2.63 m s^{-1} (or by 4.6%) and 2.52 m s^{-1} (or by 5.9%) averaged over the Arabian Sea and 1.32 m s^{-1} (or by 2.0%) and 2.41 m s^{-1} (or by 4.86%) averaged over the Bay of Bengal during the TC season and summer monsoon season, respectively.

[13] An important feature is the significant increase in PI in response to the doubled CO_2 in May when the background PI is already high, indicating that there might be stronger severe TCs in May over the North Indian Ocean as a result of global warming. Another important feature is the potentially longer TC season in the North Indian Ocean. In both June and September, the vertical shear decreases considerably and becomes below 20 m s^{-1} in response to the doubled CO_2, leading to a significant increase in dynamical efficiency and PI of TCs. As a result, the TC season is likely to become longer in a warmed climate in the North Indian Ocean. Although there are uncertainties in both the CGCM simulations in response to global warming and the calculation of the semi-empirical TC PI in this study, our results regarding to the potentially more intense TCs and possible longer TC seasons seem to be consistent with recent observational studies by *Rao et al.* [2008] and *Elsner et al.* [2008].

[14] **Acknowledgments.** This work is supported by Chinese National Science Foundation (40775060), Ministry of Science and Technology of China (GYHY200806009), Jiangsu Education Science Foundation (07KJB170065), Jiangsu Government Scholarship for Overseas Studies, China Academy of Meteorological Sciences Severe Weather National Key Laboratory 2007 Open Fund (2007LASW09), and US NSF grants ATM-0427128 and ATM-0754029 and ONR grant 000-14-06-10303 awarded to University of Hawaii. Additional support has been provided by JAMSTEC of Japan, NASA, and NOAA through their sponsorships of the International Pacific Research Center (IPRC) in School of Ocean and Earth Science and Technology (SOEST) at University of Hawaii. This is the IPRC publication IPRC-533.

References

Bister, M., and K. A. Emanuel (1998), Dissipative heating and hurricane intensity, *Meteorol. Atmos. Phys.*, *65*, 233–240.

Bister, M., and K. A. Emanuel (2002), Low frequency variability of tropical cyclone potential intensity: 1. Interannual to interdecadal variability, *J. Geophys. Res.*, *107*(D24), 4801, doi:10.1029/2001JD000776.

Elsner, J. B., J. P. Kossin, and T. H. Jagger (2008), The increasing intensity of the strongest tropical cyclones, *Nature*, *455*, 92–95.

Emanuel, K. A. (1999), Thermodynamic control of hurricane intensity, *Nature*, *401*, 665–669.

Emanuel, K. A. (2007), Environmental factors affecting tropical cyclone power dissipation, *J. Clim.*, *20*, 5497–5509.

Free, M., M. Bister, and K. A. Emanuel (2004), Potential intensity of tropical cyclones: Comparison of results from radiosonde and reanalysis data, *J. Clim.*, *17*, 1722–1727.

Rao, V. B., C. C. Ferreira, S. H. Franchito, and S. S. V. S. Ramakrishna (2008), In a changing climate weakening tropical easterly jet induces more violent tropical storms over the north Indian Ocean, *Geophys. Res. Lett.*, *35*, L15710, doi:10.1029/2008GL034729.

Tonkin, H., G. J. Holland, N. Holbrook, and A. Henderson-Sellers (2000), An evaluation of thermodynamic estimates of climatological maximum potential tropical cyclone intensity, *Mon. Weather Rev.*, *128*, 746–762.

Vecchi, G. A., and B. J. Soden (2007), Increased tropical Atlantic wind shear in model projections of global warming, *Geophys. Res. Lett.*, *34*, L08702, doi:10.1029/2006GL028905.

Webster, P. J., G. J. Holland, J. A. Curry, and H. R. Chang (2005), Changes in tropical cyclone number, duration, and intensity in a warming environment, *Science*, *309*, 1844–1846.

Zeng, Z., Y. Wang, and C.-C. Wu (2007), Environmental dynamical control of tropical cyclone intensity—An observational study, *Mon. Weather Rev.*, *135*, 38–59.

Y. Wang, International Pacific Research Center and Department of Meteorology, School of Ocean and Earth Science and Technology, University of Hawaii at Manoa, POST 409G, 1680 East West Road, Honolulu, HI 96822, USA. (yuqing@hawaii.edu)

J. Yu, Pacific Typhoon Research Center, KLME, Nanjing University of Information Science and Technology, Nanjing 210044, China.